

## Dynamic far-field fluorescence nanoscopy

This article has been downloaded from IOPscience. Please scroll down to see the full text article.

2007 New J. Phys. 9 435

(<http://iopscience.iop.org/1367-2630/9/12/435>)

View [the table of contents for this issue](#), or go to the [journal homepage](#) for more

### Download details:

IP Address: 38.107.179.226

The article was downloaded on 29/05/2012 at 11:26

Please note that [terms and conditions apply](#).

## Dynamic far-field fluorescence nanoscopy

V Westphal<sup>1</sup>, M A Lauterbach<sup>1</sup>, A Di Nicola and S W Hell<sup>2</sup>

Department of NanoBiophotonics, Max Planck Institute for Biophysical Chemistry, 37077 Göttingen, Germany  
E-mail: [shell@gwdg.de](mailto:shell@gwdg.de)

*New Journal of Physics* **9** (2007) 435

Received 29 October 2007

Published 5 December 2007

Online at <http://www.njp.org/>

doi:10.1088/1367-2630/9/12/435

**Abstract.** We demonstrate far-field fluorescence microscopy with subdiffraction resolution of rapidly moving nanoparticles. Fast recording on the nanoscale is accomplished by merging rapid beam scanning with stimulated emission depletion (STED) microscopy. By recording at 80 frames per second with a focal spot area which is 9–10-fold smaller than the diffraction limit, the Brownian motion of a dense suspension of 36 nm particles was revealed. Individual particles were localized with  $\sim 20$  nm accuracy, while automated particle tracking revealed their distribution of speeds. The first combination of rapid image acquisition with a diffraction-unlimited far-field microscopy concept heralds a large range of possible applications of dynamic fluorescence nanoscopy in various fields, including in biology.

<sup>1</sup> Both authors contributed equally to this work.

<sup>2</sup> Author to whom any correspondence should be addressed.

**Contents**

<b>1. Introduction</b>	<b>2</b>
<b>2. STED microscopy</b>	<b>2</b>
<b>3. Sample preparation</b>	<b>4</b>
<b>4. Resolution quantification</b>	<b>5</b>
<b>5. Dynamic imaging</b>	<b>5</b>
<b>6. Localization and tracking</b>	<b>7</b>
<b>7. Particle speeds</b>	<b>7</b>
<b>8. Discussion and conclusion</b>	<b>8</b>
<b>Acknowledgments</b>	<b>9</b>
<b>References</b>	<b>9</b>

**1. Introduction**

For more than a century it has been widely acknowledged that the resolution of any lens-based (far-field) optical microscope is limited by diffraction to  $\lambda/(2n\sin\alpha)$ , with  $\lambda$  denoting the wavelength of light,  $n$  the index of refraction, and  $\alpha$  the semiaperture angle of the lens. However, for the important contrast mode of fluorescence imaging, physical concepts have emerged that overcame the diffraction barrier by judiciously incorporating the fluorophore properties in the image formation [1]–[3]. The first viable concept is stimulated emission depletion (STED) microscopy [4] yielding a scanning microscope whose effective point spread function (PSF) (i.e. focal fluorescent spot) can theoretically be reduced down to the size of a molecule [2]. Providing spatial resolutions of 16–80 nm [5, 6], practical STED microscopy has revealed a gamut of features that were hitherto not accessible by focused visible light. Specifically, STED microscopy has been used to unravel protein agglomerations on the nanoscale inside cells [6] and on cell membranes [7]–[10], while outside biology it has been used to image nanoparticle assemblies [8] and nanolithography structures [11]. However, STED and in fact all fluorescence nanoscopy imaging techniques so far described [3], [12]–[14] have been applied only to static samples. Moving structures demand faster recording which is connected with fewer photons acquired per image. But apart from this, there is no reason why far-field optical nanoscopy of dynamic objects would be precluded [3]. We have hence developed a rapidly scanning STED microscope that records 80 frames per second (fps), i.e. three times the video rate. The unique combination of speed and subdiffraction resolution is applied to visualize and quantify the Brownian motion in a highly concentrated suspension of 36 nm particles that, to our knowledge, is currently not measurable by any other method. The nanoresolution movies gained by STED were directly compared with their diffraction-limited counterparts recorded in a high-end confocal mode [15]. Our results provide the first practical evidence that far-field optical nanoscopy of highly dynamic samples is possible.

**2. STED microscopy**

The principles of STED microscopy have been described in detail elsewhere [4, 5, 8, 16]. In brief, STED microscopy is usually performed with an ordinary beam for exciting the marker

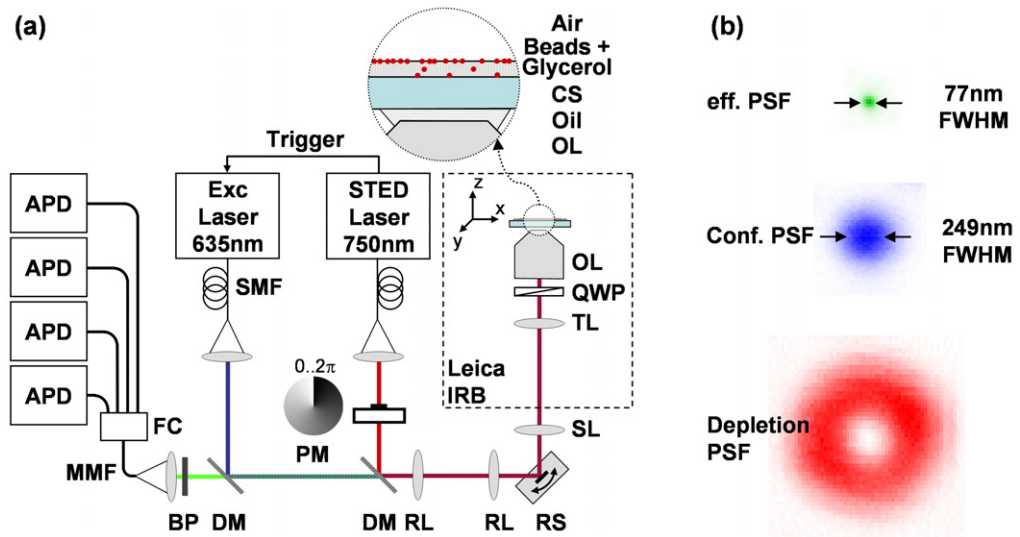


**Figure 1.** (a) Set-up of a beam scanning STED microscope based on a standard microscope body (Leica IRB). The blowup sketches the sample to be imaged. (b) Applying the doughnut-shaped depletion point-spread-function (PSF) on top of the confocal PSF yields an effective PSF of the STED microscope whose maximum is reduced  $\sim 3.2$ -fold in diameter and hence by 10-fold in focal area. The effective PSF has been measured by imaging 17 static fluorescent beads of 20 nm diameter. The sharpened effective PSF leads to images of higher resolution. Abbreviations: APD, avalanche photo diode; MMF, multimode fiber; FC, fiber coupler; BP, band pass filter; DM, dichroic mirror; Exc, excitation; SMF, single mode fiber; PM, phase mask; RL, relay lens; RS, resonant scanner; SL, scan lens; TL, tube lens; QWP, quarter wave plate; OL, objective lens and CS, cover slip.

molecules from the ground state ( $S_0$ ) to the fluorescent state ( $S_1$ ), co-aligned with a wavefront-modified beam producing a doughnut-shaped focal spot (figure 1(b)) which depletes the  $S_1$  by stimulated emission. The wavelength of this depletion (STED) beam is located at the red edge of the emission spectrum of the fluorophore. The fluorescence is recorded from the remaining part of the emission spectrum. Depletion of the  $S_1$  outside the central zero of the doughnut confines the occurrence of the  $S_1$ , and hence the ability of a molecule to fluoresce, to a smaller area. The FWHM of this spot, i.e. the effective PSF of the microscope, follows  $d \approx \lambda / (2n \sin \alpha \sqrt{1 + I/I_s})$ . The variable  $I$  is the intensity of the STED-beam at the doughnut crest whereas  $I_s$  denotes a dye-characteristic intensity [2, 5]. The scanning of this spot across the sample and registering the fluorescence renders subdiffraction images. By allowing  $I/I_s \rightarrow \infty$  it follows that  $d \rightarrow 0$ . Therefore, the spatial resolution can ideally be improved up to the molecular scale [2, 5, 6, 17]. In any case, the size of the fluorescent spot  $d$  can be tuned by adjusting  $I/I_s$ , a phenomenon which allows one to weigh the benefit of having a larger fluorescence photon flux against resolution.

To ease sample handling, the set-up shown in figure 1(a) was built around an inverted microscope stand (IRB, Leica, Heidelberg, Germany). A slight modification of the microscope stand gave access to its optical path from the bottom. Both excitation and STED were performed

with synchronized trains of pulses. The excitation pulses of 120 ps duration as provided by a triggerable laser diode (LDH-P-635, PicoQuant, Berlin, Germany) at  $\lambda = 635$  nm were swiftly followed by up-chirped STED pulses of 300 ps duration, originally stemming from a 120 fs mode-locked Ti:sapphire laser (MaiTai, Newport, Irvine, CA) with  $\lambda = 750$  nm as center wavelength. After passing single mode fibers, the beams were combined with a dichroic mirror. They were subsequently relayed and demagnified with two achromats in a 4f-configuration. Beam scanning along the  $x$ -axis was performed with a 16 kHz resonant mirror (SC-30, EOPC, Glendale, NY), whereby the original scan and tube lens of the microscope acted as a second relay pair. A quarter wave plate ensured circular polarization of the beams entering the objective lens (NA = 1.4 oil immersion, HCX PL AP, Leica). The focal intensities for excitation and STED amounted to  $6.5 \text{ MW cm}^{-2}$  and  $I \approx 400 \text{ MW cm}^{-2}$ , respectively. With  $I_s \approx 30 \text{ MW cm}^{-2}$  which was determined in previous experiments [18], we expected a FWHM reduction of  $\sim 3.5$ -fold.

The fluorescence was collected by the objective lens and after descanning it was separated from the incoming beams using dichroic mirrors. A bandpass filter ( $675 \pm 30$  nm, AHF, Tübingen, Germany) removed scattered light. The set-up was confocalized by imaging the fluorescence on the aperture of a multimode fiber featuring an opening diameter of 0.7 times the backprojected Airy disc of a diffraction-limited spot. To enable high count rates, the fluorescence was divided with a 1:4 fiber coupler onto four avalanche photo diodes (APDs, SPCM-AQR13, Perkin Elmer, Fremont, CA) featuring  $> 65\%$  quantum efficiency of detection. The resulting bright images enabled high frame rates. Photon counting and data-preprocessing were accomplished with a custom field programmable gate array board.

The focal doughnut was realized by placing a vortex phase plate (VPP-A1, RPC Photonics, NY) in the collimated STED beam path. Produced as a polymer replica on a glass substrate, this phase mask greatly simplified the doughnut production as compared to the spatial light modulators previously employed [6]–[8]. Special care was taken to properly align the axial position of the resonant mirror so that lateral movements of the image of the phase mask across the back aperture of the objective lens are prevented. The  $y$ - and  $z$ -scanning of the sample was provided by a piezo stage (733-3DD and E-710, Physik Instrumente GmbH, Karlsruhe, Germany) featuring a digital piezo controller with an internal feedback loop. The feedback loop minimized scan errors during rapid, repetitive scanning, thereby allowing bidirectional frame acquisition at 80 fps. The images were sampled with 30 nm pixel size in both dimensions, i.e. slightly below the Nyquist limit (35 nm).

### 3. Sample preparation

To quantify the effective PSF, we utilized a sample of fixed 20 nm diameter fluorescent beads (Crimson, InvitroGen, Carlsbad, CA) embedded in PVA, spincoated onto a glass cover slip. Moreover, a sample with rapidly diffusing beads was prepared by first thoroughly cleaning the cover slips with the detergent Mucosol and making their surface hydrophilic in a plasma cleaner (Diener Electronic, Nagold, Germany). The surfaces of the cover slips were then passivated with 1 M NaOH. Later,  $6 \mu\text{l}$  of 36 nm fluorescent bead suspension (approx. 4% w/v, actual size according to manufacturer  $36 \pm 5$  nm, Crimson, InvitroGen) were mixed with  $200 \mu\text{l}$  glycerol and  $1 \mu\text{l}$  of 10 M NaOH and then spincoated onto these cover slips at 8000 rpm. The spincoating for 1 min resulted in  $1\text{--}2 \mu\text{m}$  thick films. The beads were mostly confined to the glycerol surface, forming a two-dimensional (2D) sample simplifying particle tracking. The density of particles varied across the sample.

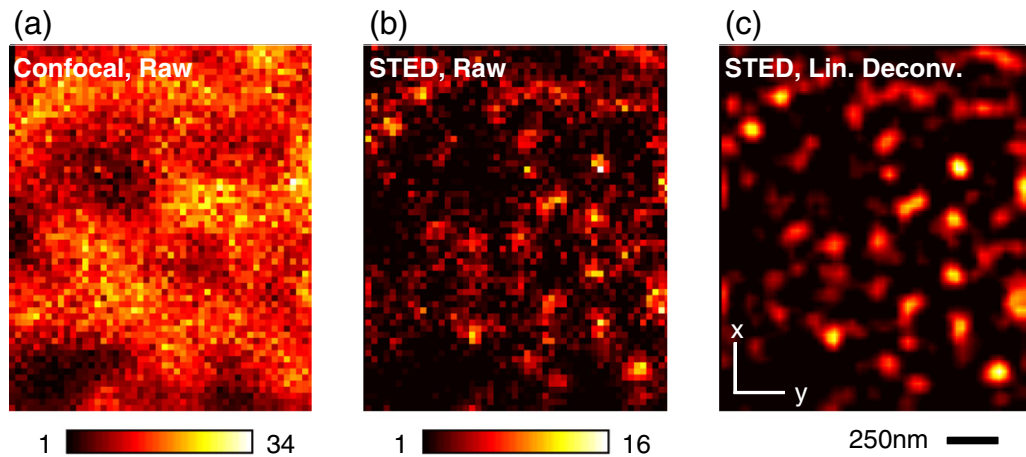


**Figure 2.** Individual images (i.e. single frames) of fluorescent 36 nm beads in glycerol recorded at 80 fps: (a) confocal and (b) STED. (c) Linear deconvolution with the effective PSF of the STED microscope. The frame acquisition time was 10 ms, with 2.6 ms used for reversal of the scan direction. With  $60 \times 50$  pixels per frame, the pixel dwell time was  $1.9 \mu\text{s}$ . See also movie 1. The colorbars indicate the photon counts per pixel.

#### 4. Resolution quantification

To determine the effective PSF or spot size of the STED microscope under the applied parameters of operation, we imaged 20 nm beads fixed in PVA with a pixel dwell time of  $150 \mu\text{s}$  and a pixel size of 15 nm. Images of individual beads were manually identified and averaged. Specifically, 17 and 5 bead images were evaluated for the STED and the confocal mode, respectively. In the STED mode, the measured FWHM of the effective focal spot was 77 and 74 nm for  $x$  and  $y$ , respectively (figure 1(b)). In the glycerol sample containing the rapidly diffusing beads, the FWHM of individual spots was predicted as 83 and 80 nm, for  $x$  and  $y$ , respectively, due to the slightly larger particle diameter of 36 nm. Nonetheless, comparison with the confocal FWHM of 249 nm (measured on the fixed beads) revealed an  $\sim 3$ -fold reduction in FWHM. The average background originating from stray light, measured with a blank sample, amounted to 0.3 counts per pixel, which can be neglected.

#### 5. Dynamic imaging

Figure 2 compares individual frames representing 10 ms snapshots of rapidly diffusing 36 nm beads, by confocal and STED microscopy. STED but not confocal microscopy was capable of capturing individual diffusing particles. In fact, the confocal mode failed to identify individual beads throughout the whole time series. The application of a linear deconvolution (Wiener filtering) for visualization employing the effective PSF of the STED microscope acted as a noise filter (figure 2(c)) while preserving the resolution in the image. Importantly, the images are excerpts of nanoscopy movies that were taken consecutively from the sample (figure 3). The movie provided in the supplementary information demonstrates the dramatic increase in information conveyed by the STED mode; see movie 1.

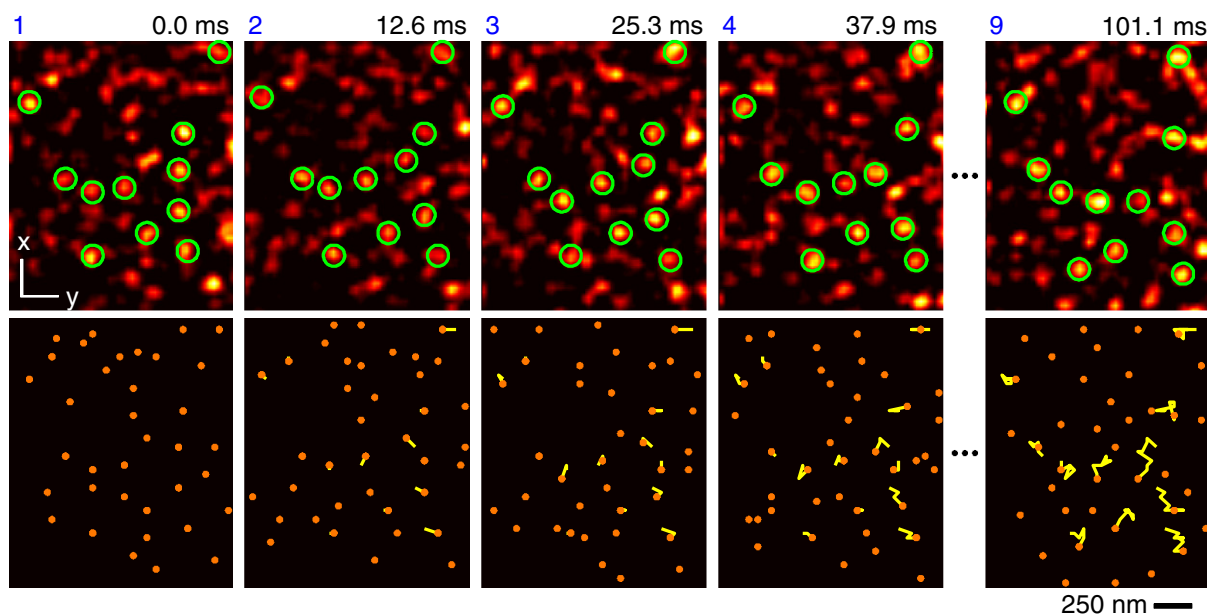


**Figure 3.** Rapidly diffusing 36 nm diameter fluorescent particles in a glycerol film shown in subsequent frames recorded at 80 fps; data shown after linear deconvolution (upper panels). Some particles are marked to highlight their movement. All positions at which particles were identified are marked by orange dots of 36 nm diameter (lower panels). Yellow traces show the movement of the particles marked in the upper panels. The 250 nm scalebar also indicates the resolution limit of a corresponding confocal system. See also movie 1.

**Movie 1.** Available from [stacks.iop.org/njp/9/435/mmedia](http://stacks.iop.org/njp/9/435/mmedia). 36 nm nanoparticles diffusing in a glycerol film imaged at 80 fps, displayed with only 30 fps, to simplify perception. The first 100 frames were captured with confocal microscopy resolution. The remainder was recorded in the subdiffraction STED-mode featuring a focal spot area reduced by 9-fold over confocal microscopy. From left to right, the panels display the raw data, a linear deconvolution using the PSF of the respective recording mode, and the identified particle positions. Exemplary traces are marked in the data exhibiting the individual particle positions. The high density of particles precludes the identification of individual particles in the confocal mode, even after linear deconvolution. In contrast, STED microscopy clearly discerned rapidly diffusing particles.

The doughnut shape of the focus and the rapid scanning suppresses trapping of the nanoparticles by the STED beam, despite its  $\sim 28$  mW time-averaged power. Nevertheless, we initially observed in some preparations, that particles gradually left the field-of-view, when the STED beam was switched on. As this presumably was due to high water content in the glycerol films, we could avoid this effect by preparing the sample with dry glycerol. Another potential remedy is to use fluorophores with lower  $I_s$  requiring lower STED-beam power.

## 6. Localization and tracking

To allow automatic localization and tracking we implemented a simple algorithm that was first tested and optimized using a Monte Carlo simulation. The simulation assumed a Poissonian brightness distribution of 100 counts per particle, which is of the order of the 50–250 counts per particle measured. On average 70 beads were assumed in each image at random positions. To find an optimal tradeoff between a high probability to recognize particles and a low probability of false positives, we systematically tested different parameters, such as the width of the smoothing function, the regularization in the employed deconvolution, and the threshold. The best results for localization and tracking were achieved by smoothing with a Cauchy–Lorentz function of 120 nm FWHM which is slightly broader than the FWHM of the effective PSF, owing to the signal-to-noise ratio in the raw data. The bead positions were determined by identifying their local maxima and subsequently refining the data to sub-pixel precision by fitting. Maxima with brightness <10% of the brightest object in the smoothed image series were discarded. Individual particles were tracked using the algorithm described by Crocker and Grier [19], as implemented by Blair and Dufresne in Matlab (<http://physics.georgetown.edu/matlab/>). In brief, the squared distance between all selected particles in consecutive frames was minimized, constrained to a maximal speed of 10–24 nm ms<sup>-1</sup> (4–10 pixel per frame), depending on the sample density.

## 7. Particle speeds

As a next step we quantified the distribution of the particle speeds. The speed of individually tracked particles was calculated as  $v = \Delta x_{\text{frame}} / \Delta t_{\text{frame}}$  with  $\Delta x_{\text{frame}}$  denoting the displacement of the particle from frame to frame, and with  $\Delta t_{\text{frame}} = 12.6$  ms being the time difference between two frames. In this experiment the particle density was nine times lower than in the sample of figures 2 and 3, because this ensured that the maximal displacement of the particles between two frames was smaller than the average particle density. The speed histogram of  $\sim 35\,000$  speed measurements taken from 2100 traces of individually resolved beads revealed close correspondence to a  $\chi$ -distribution with two degrees of freedom describing 2D particle diffusion in space [20]:

$$v \, dv = \beta v \exp \left[ -\frac{\beta v^2}{2} \right] dv. \quad (1)$$

The constant  $\beta$  depends on the medium viscosity and on the particle diameter. Figure 4 shows that a single parameter fit to the measured distribution matches well for  $\beta = 0.33$ . The vast majority of speeds was significantly <24 nm ms<sup>-1</sup> which was the maximum speed that could be tracked at this particle density. Fitting of equation (1) to the measured speed distribution gave a peak at 4.2 nm ms<sup>-1</sup>. The standard deviation of bead displacement  $\sqrt{\langle \Delta x^2 \rangle}$  after  $\Delta t$  can be used to estimate the resolution degradation due to motion artifacts. The data underlying figure 4 yield  $\sqrt{\langle \Delta x_{\text{frame}}^2 \rangle} = 72$  nm between two frames. Meanwhile, relevant for the blurring of a single particle is the time  $\Delta t_{\text{bead}}$  required to record a particle. Because we imaged every particle with five subsequent line scans,  $\Delta t_{\text{bead}}$  equaled  $5 \times 0.2$  ms = 1 ms. Since  $\sqrt{\langle x^2 \rangle}$  scales with  $\sqrt{\Delta t}$ ,  $\sqrt{\langle \Delta x_{\text{bead}}^2 \rangle} = 20$  nm, which can be neglected at a spot size of  $\sim 80$  nm.

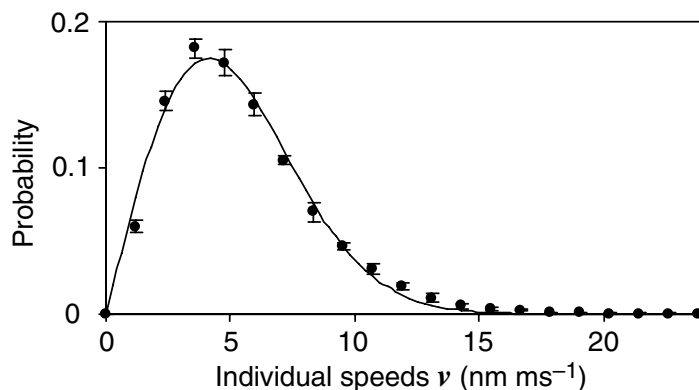


**Figure 4.** Comparison of the measured speed distribution (dots) of diffusing nanoparticles with the fitted  $\chi$ -distribution (line) describing 2D-particle diffusion. Error bars are the standard error of the mean between different data sets.

## 8. Discussion and conclusion

Since the diffuse background is negligible in our recordings, the localization precision of a nanoparticle is determined by  $d/\sqrt{N}$  with  $N$  denoting the number of photons in the spot. The reduction of the spot FWHM by a factor of  $m$  in STED over confocal microscopy requires the sample to be scanned  $m$  times finer both in the  $x$ - and in the  $y$ -direction. Given the same sampling density, confocal recording yields  $m^2$  more photons than its STED counterpart, but at an  $m$  times larger spot diameter. Therefore, the localization precision in the confocal mode, given by  $(dm)/\sqrt{Nm^2}$ , is the same as that in the STED mode. Although the localization precision of individual particles remains unchanged, STED yields the same localization precision in  $m^2$  times denser samples.

STED microscopy does not require any computation for attaining the improved resolution since the resolution improvement is purely physical in nature. The effective PSF of a STED microscope just describes the probability that a certain focal coordinate contributes to the signal measured at the detector. Scanning this effective PSF across the specimen implies that each point in the sample is evenly covered. This is tantamount to a linear image formation, with the image being given by the convolution of the effective PSF with the local concentration of marker molecules. STED recording inherently ensures that apart from shot noise, the brightness in the image is proportional to the local marker density.

In these initial experiments, we applied only a single local zero in the focal STED intensity distribution, but STED microscopy could be parallelized by means of arrays of zeros [2]. The zeros can be as close as allowed by the diffraction resolution limit, because larger distances can be well separated in any diffraction-limited system. Parallelization with arrays of zeros can be implemented either with the concomitant arrays of point detectors or with a camera recording in a ‘widefield’ mode [2, 3]. Another strategy to increase the imaging speed is to restrict recording to single line scanning, which is viable for a number of applications. STED microscopy can be extended to 3D [18, 21] by quenching fluorescence above and below the focal plane by a suitably shaped STED beam. Scanning a volume instead of a plane reduces, of course, the time resolution by the number of planar scans used to sample the volume. However, an important feature of STED nanoscopy is that the recording can be arbitrarily targeted to any coordinate

in space. In a suitable technical implementation, the STED-beam could also follow 3D trajectories.

The obtained fluorescence signal can be increased 2-fold by collection with two objectives in a 4Pi configuration [22, 23] which would double the number of detected photons or even further improve the axial resolution. Another option to improve the fluorescent photon flux is to implement STED with continuous wave beams [18]. For dyes with a low triplet state yield, the absence of interpulse breaks in continuous wave illumination is expected to increase the signal over the current 80 MHz pulsing scheme. Relying on their properties, the performance of STED microscopy will correlate with the performance of the fluorophores in use. Therefore, further improvements can be anticipated from improving the fluorophores with regard to signal and photostability.

While rapid nanoscale recording reduces the collected signal per image, the challenges posed by decreased signal should not be overestimated. In fact the lower panels in figure 3 show that with the focal spot size reaching the size of features to be discerned, one can use the information about these features for their recognition. The use of such information reduces the signal required to identify individual features, because the function describing the object sought after becomes a discrete distribution of known particles. Consequently, we expect that the combination of nanoscale resolution with *a priori* information from (the discrete size distribution of) these particles will help in reducing the demands on the signal.

Therefore, in the future, data analysis algorithms that are more elaborate than the simple one used herein, will improve the identification and localization of individual features in the image. They can make use of the photon count statistics and infer information from neighboring images in the time series. Upcoming applications of this novel high-speed, super-resolution imaging instrument will also include live cells. In this scenario, the observation of dense distributions of sub-diffraction-sized structures should have a substantial impact in cell biology. In fact, initial experiments in our laboratory have evidenced the viability of nanoscale live cell STED applications with imaging speeds of several frames per second.

In conclusion, we have demonstrated rapid far-field optical microscopy of highly dynamic samples at more than three times the video rate, and a focal spot area that is  $\sim 10$ -fold below the diffraction barrier. Our results mark the advent of optical microscopy imaging of densely labeled samples with high speed and nanoscale resolution using regular lenses and visible focused light.

## Acknowledgments

We thank J Keller for helpful discussions on particle localization and A Schönle for his data acquisition software 'ImSpector' and for help with the necessary hardware drivers. We acknowledge E Rittweger and J Jethwa for carefully reading the manuscript.

## References

- [1] Hell S W 1994 *Opt. Commun.* **106** 19–24
- [2] Hell S W 2003 *Nat. Biotechnol.* **21** 1347–55
- [3] Hell S W 2007 *Science* **316** 1153–8
- [4] Hell S W and Wichmann J 1994 *Opt. Lett.* **19** 780–2
- [5] Westphal V and Hell S W 2005 *Phys. Rev. Lett.* **94** 143903

- [6] Donnert G, Keller J, Medda R, Andrei M A, Rizzoli S O, Lührmann R, Jahn R, Eggeling C and Hell S W 2006 *Proc. Natl Acad. Sci. USA* **103** 11440–5
- [7] Willig K I, Rizzoli S O, Westphal V, Jahn R and Hell S W 2006 *Nature* **440** 935–9
- [8] Willig K, Keller J, Bossi M and Hell S W 2006 *New J. Phys.* **8** 106
- [9] Sieber J J, Willig K I, Heintzmann R, Hell S W and Lang T 2006 *Biophys. J.* **90** 2843–51
- [10] Sieber J J *et al* 2007 *Science* **317** 1072–6
- [11] Westphal V, Seeger J, Salditt T and Hell S W 2005 *J. Phys. B: At. Mol. Opt. Phys.* **38** S695–S705
- [12] Gustafsson M G L 2005 *Proc. Natl Acad. Sci. USA* **102** 13081–6
- [13] Betzig E, Patterson G H, Sougrat R, Lindwasser O W, Olenych S, Bonifacino J S, Davidson M W, Lippincott-Schwartz J and Hess H F 2006 *Science* **313** 1642–5
- [14] Bates M, Huang B, Dempsey G P and Zhuang X 2007 *Science* **317** 1749–53
- [15] Wilson T and Sheppard C J R 1984 *Theory and Practice of Scanning Optical Microscopy* (New York: Academic)
- [16] Klar T A, Engel E and Hell S W 2001 *Phys. Rev. E* **64** 066613
- [17] Hell S W 1997 *Increasing the Resolution of Far-Field Fluorescence Light Microscopy by Point-Spread-Function Engineering (Topics in Fluorescence Spectroscopy vol 5)* ed J R Lakowicz (New York: Plenum) pp 361–422
- [18] Willig K, Harke B, Medda R and Hell S W 2007 *Nat. Methods* **4** 915–8
- [19] Crocker J C and Grier D G 1996 *J. Colloid Interface Sci.* **179** 298–310
- [20] Einstein A 1905 *Ann. Phys. Lpz.* **17** 549–60
- [21] Klar T A, Jakobs S, Dyba M, Egner A and Hell S W 2000 *Proc. Natl Acad. Sci. USA* **97** 8206–10
- [22] Lang M, Müller T, Engelhardt J and Hell S W 2007 *Opt. Express* **15** 2459–67
- [23] Hell S and Stelzer E H K 1992 *J. Opt. Soc. Am. A* **9** 2159–66